Appendix A: Bayesian statistical model

Taking into account the uncertainties in the equation of state, the temperature at 1 bar, the pressure where helium-rain happens, and the error bars on the measurements themselves, we employed a Bayesian statistical approach to explore a large ensemble of Jupiter models and find which are the possible scenarios for Jupiter's internal structure that fit all observational constraints. The parameters of CEPAM we allowed to vary are

$$\boldsymbol{\theta} = \begin{cases} [M_{core}, Z_2^{\rm rock}, Z_2^{\rm ice}, T_{\rm 1bar}, P_{\rm He}, \Delta T_{\rm He}] & \text{three-layer} \\ [M_{core}, Z_{\rm dilute}^{\rm rock}, Z_{\rm dilute}^{\rm ice}, m_{\rm dilute}, T_{\rm 1bar}, P_{\rm He}, \Delta T_{\rm He}] & \text{dilute-core,} \end{cases} \tag{A.1}$$

and the data we allowed to vary are

$$\boldsymbol{X} = [J_2^{static}, J_4^{static}, J_6^{static}, J_8^{static}, J_{10}^{static}, R_{eq}^{obs}] \tag{A.2}$$

The quantity of interest is the posterior density function of the parameters that are conditional on the data, $p(\boldsymbol{\theta}|\boldsymbol{X})$. Bayes' theorem tells us that the posterior density function is completely specified by the likelihood, $p(\boldsymbol{X}|\boldsymbol{\theta})$, and the prior density function, $p(\boldsymbol{\theta})$, through the relation

$$p(\boldsymbol{\theta}|\boldsymbol{X}) \propto p(\theta) p(\boldsymbol{X}|\boldsymbol{\theta}). \tag{A.3}$$

The likelihood is the probability density of the data, which is conditional on the parameters. In general, it is not a probability density for the parameter. The prior density encodes the information we have on the parameters before the inference processes (e.g. theoretical limits and previous measurements).

It is possible, under some assumptions, to write analytical forms for the likelihood and the prior. To define the former, we first assumed an additive statistical model,

$$\boldsymbol{X} = \boldsymbol{\jmath}(\boldsymbol{\theta}) + \boldsymbol{\epsilon}. \tag{A.4}$$

Here $\boldsymbol{\jmath}$ is a mapping from the space of parameters to the space of observables. In practice, it represents our code solving the equations of planetary structure. The vector $\boldsymbol{\epsilon}$ represent a random noise. The distribution of this noise is thus the distribution of $\boldsymbol{X} - \boldsymbol{\jmath}(\boldsymbol{\theta})$. We assume now that the distribution of $\boldsymbol{\epsilon}$ is normal and that its covariance matrix is diagonal. The likelihood function is therefore

$$p(\boldsymbol{X}|\boldsymbol{\theta}) \propto \prod_i \exp\left[-\frac{(X_i - \jmath_i(\boldsymbol{\theta}))^2}{2\sigma_i^2}\right]. \tag{A.5}$$

The σ_i^2 represent the diagonal elements of the covariance matrix and are given by the observational uncertainties corresponding to the components of $\boldsymbol{X}$. The adopted values are given in Tables A.1 and A.2.

In order to simplify the prior density, we assumed that all parameters are independent. It can thus be written as the product of univariate densities,

$$p(\boldsymbol{\theta}) \propto \prod_i p_i(\theta_i). \tag{A.6}$$

The chosen priors are given in Tables A.1 and A.2. The boundaries of all priors were chosen using a test-and-trial stage, ensuring that they were wide enough to avoid numerical issues during the sampling stage and that they were narrow enough so that the parameter space to sample is not too vast.

We used an affine invariant MCMC algorithm (Christen & Fox 2010; Goodman & Weare 2010) to sample the space of parameters and to approximate the posterior probability functions. It uses the relative positions in the parameter space of several Markov chains, run in parallel, to efficiently adapt the proposition law. Using 512 walkers, we found that good convergence for the MCMC simulations can be reached with approximately 10000 iterations of the algorithm.

Figures A.1, A.2, A.3, A.4, A.5, and A.6 show the corner plots with all the parameters that result from the MCMC calculations for the six cases considered (see the main text for an extended discussion on the results).

Table A.1: Parameters explored in our MCMC calculations for three-layer models. The parameter is given in the first column, the corresponding distribution in the second, and the lower and upper bounds in the third and fourth. When relevant, the mean and the standard deviation of the truncated normal are given in columns five and six. Y_{proto}=0.277, Y_1=0.238, and Z_1=0.0153.

Parameter	Distribution	Lower bound	Upper bound	μ	σ
M_{core} (M_{Jup})	Uniform	0	0.075	–	–
$Z_2^{\rm rock}$	Uniform	0	0.5	–	–
$Z_2^{\rm ice}$	Uniform	0	0.5	–	–
$T_{\rm 1bar}$ (K)	Normal	135	215	165	4
$P_{\rm He}$ (Mbar)	Normal	0.8	9	3	0.5
$\Delta T_{\rm He}$ (K)	Uniform	0	2000	–	–

Table A.2: Parameters explored in our MCMC calculations for dilute-core models. The parameter is given in the first column, the corresponding distribution in the second, and the lower and upper bounds in the third and fourth. When relevant, the mean and the standard deviation of the truncated normal are given in columns five and six. Y_{proto} = 0.277, Y_{H_2} = 0.238, Z_1 = 0.0153, and Z_2 = 0.0153.

Parameter	Distribution	Lower bound	Upper bound	μ	σ
$M_{inner-core}$ (M_{Jup})	Uniform	0	0.075	–	–
$Z_{\rm dilute}^{\rm rock}$	Uniform	0	0.5	–	–
$Z_{\rm dilute}^{\rm ice}$	Uniform	0	0.5	–	–
$m_{\rm dilute}$	Uniform	0	0.6	–	–
$T_{\rm 1bar}$ (K)	Normal	135	215	165	4
$P_{\rm He}$ (Mbar)	Normal	0.8	9	3	0.5
$\Delta T_{\rm He}$ (K)	Uniform	0	2000	–	–

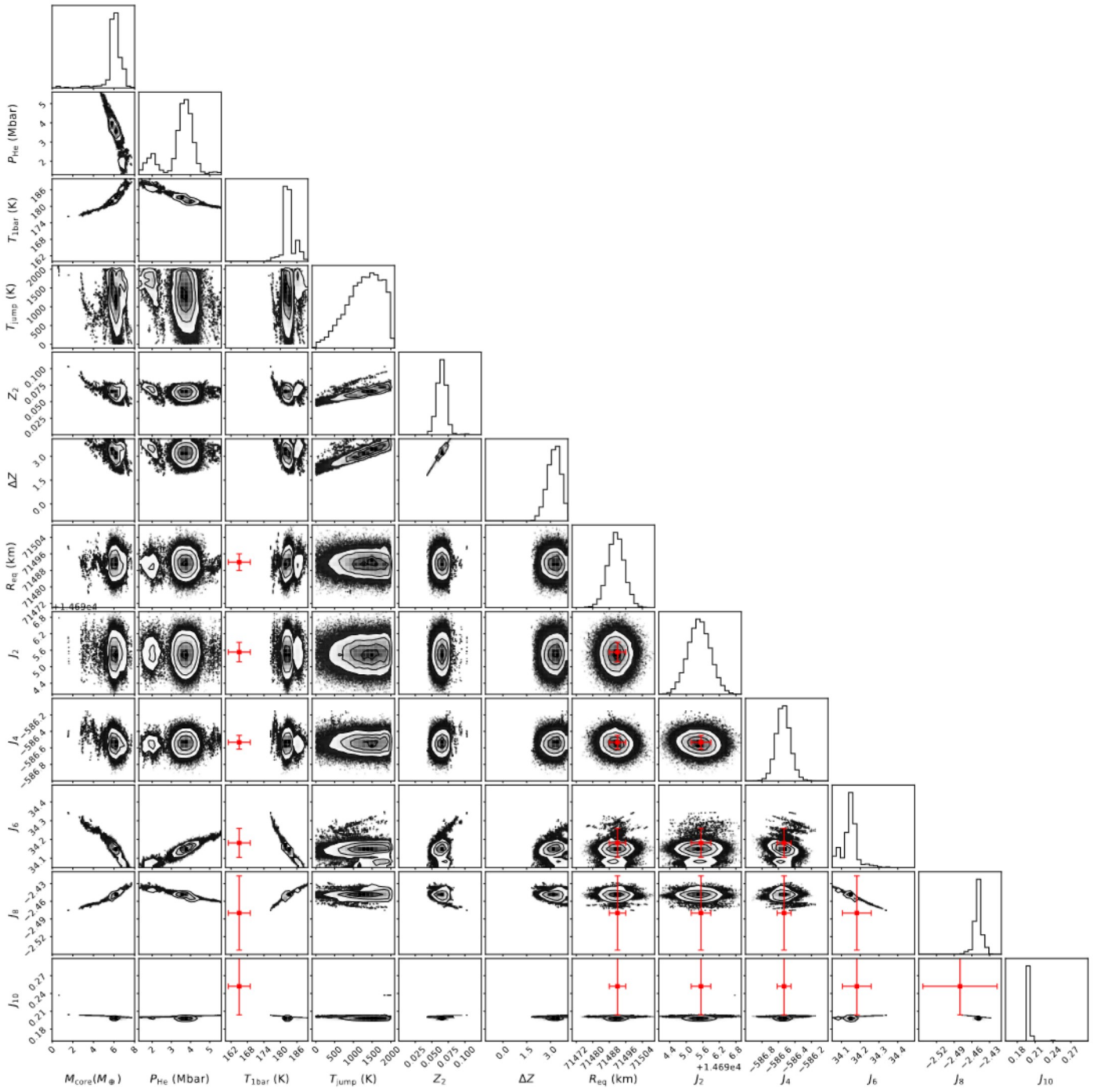

Fig. A.1: MCMC corner plot showing the posterior distribution of variables obtained with the three-layer model and the MH13 equation of state. Red points with error bars show the observed parameters as a reference.

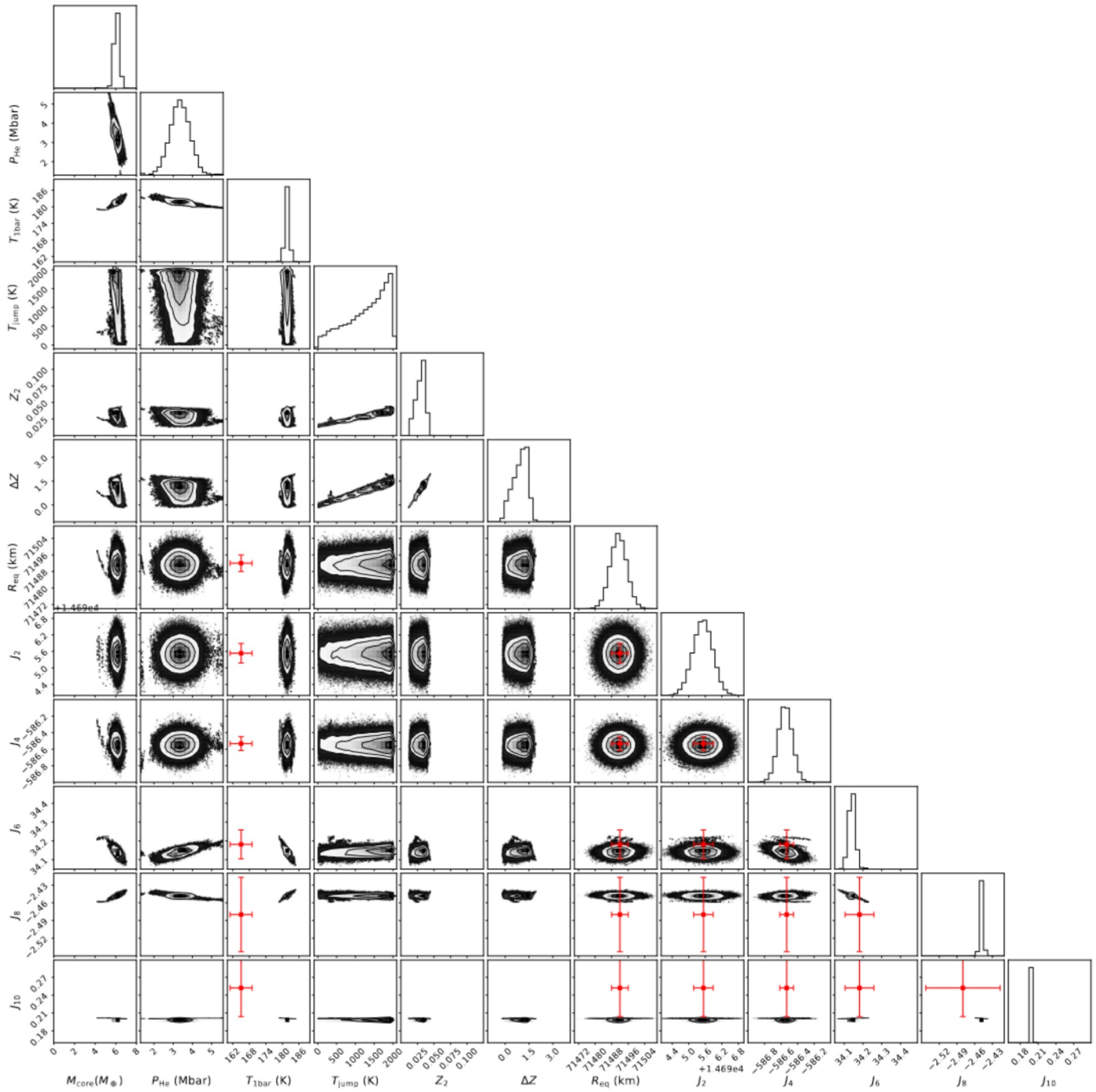

Fig. A.2: Posterior distribution results of the MCMC runs with three layers and the CMS19 equation of state. Observed parameters are indicated with the red points.

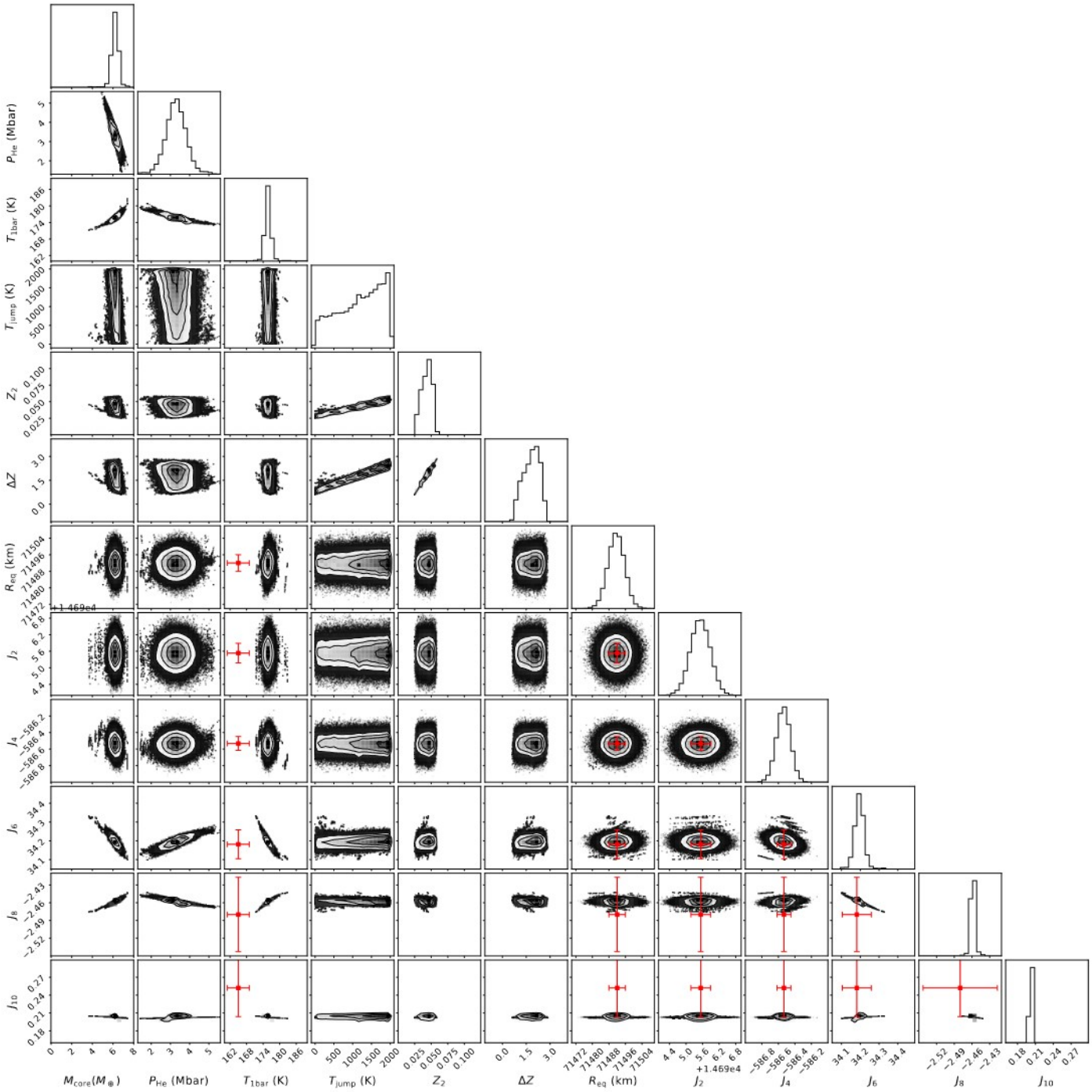

Fig. A.3: Distribution results of the MCMC runs with three layers and the MLS20 equation of state.

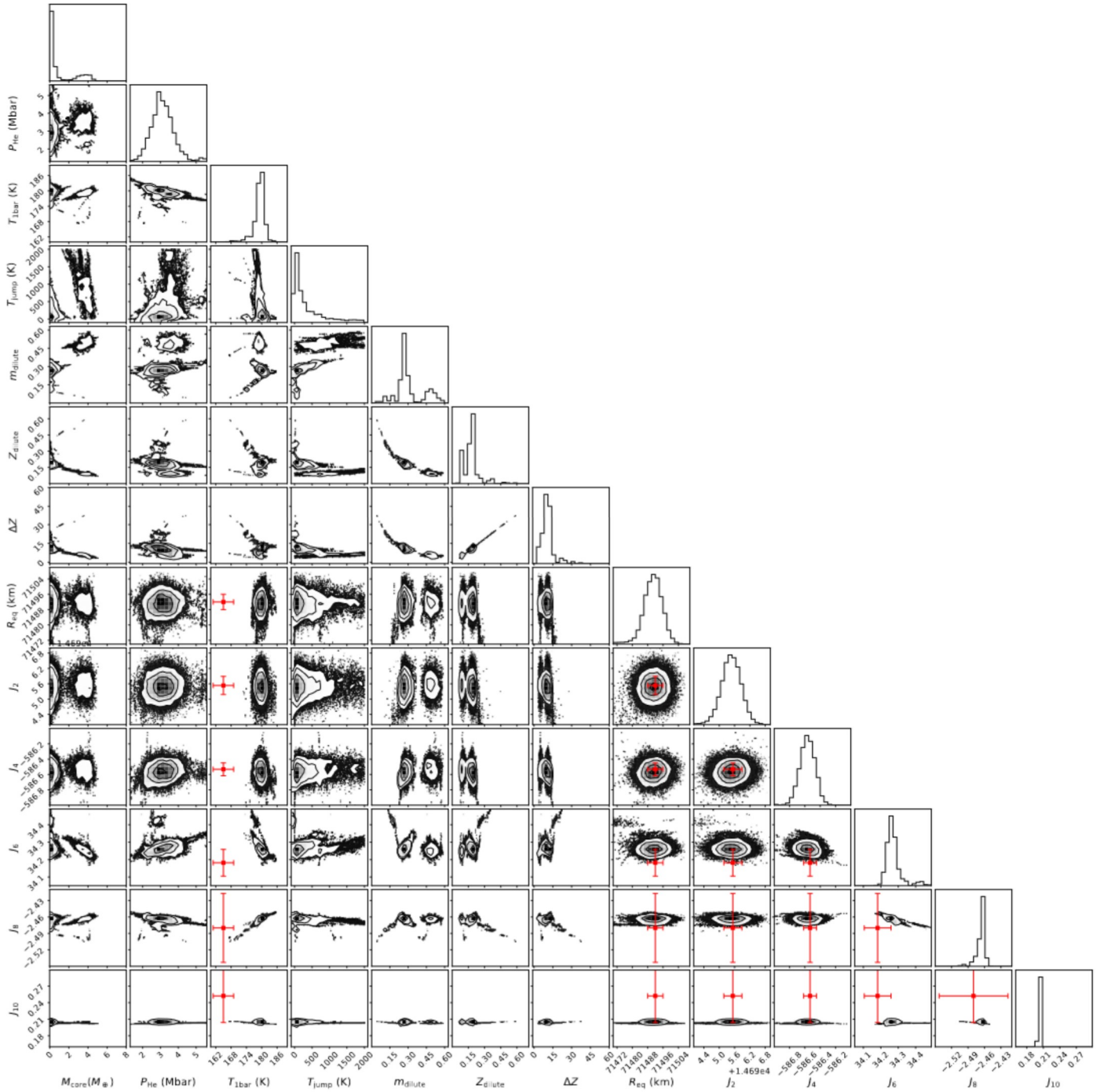

Fig. A.4: Corner plot resulting from the runs with the dilute-core model and the MH13 equation of state. Red dots show the observed parameters.

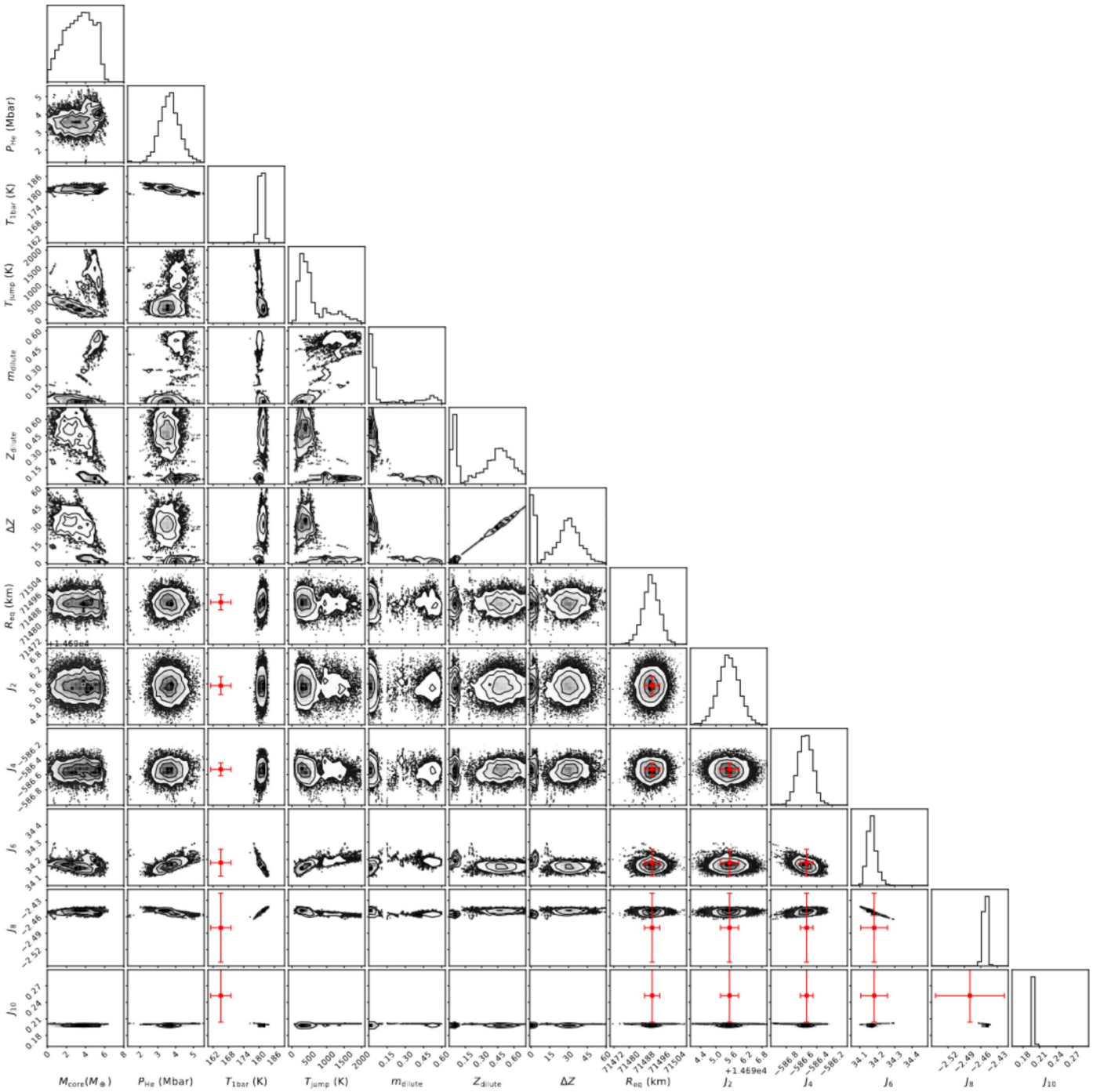

Fig. A.5: Distribution of different parameters resulting from the runs with the dilute-core model and the CMS19 equation of state.

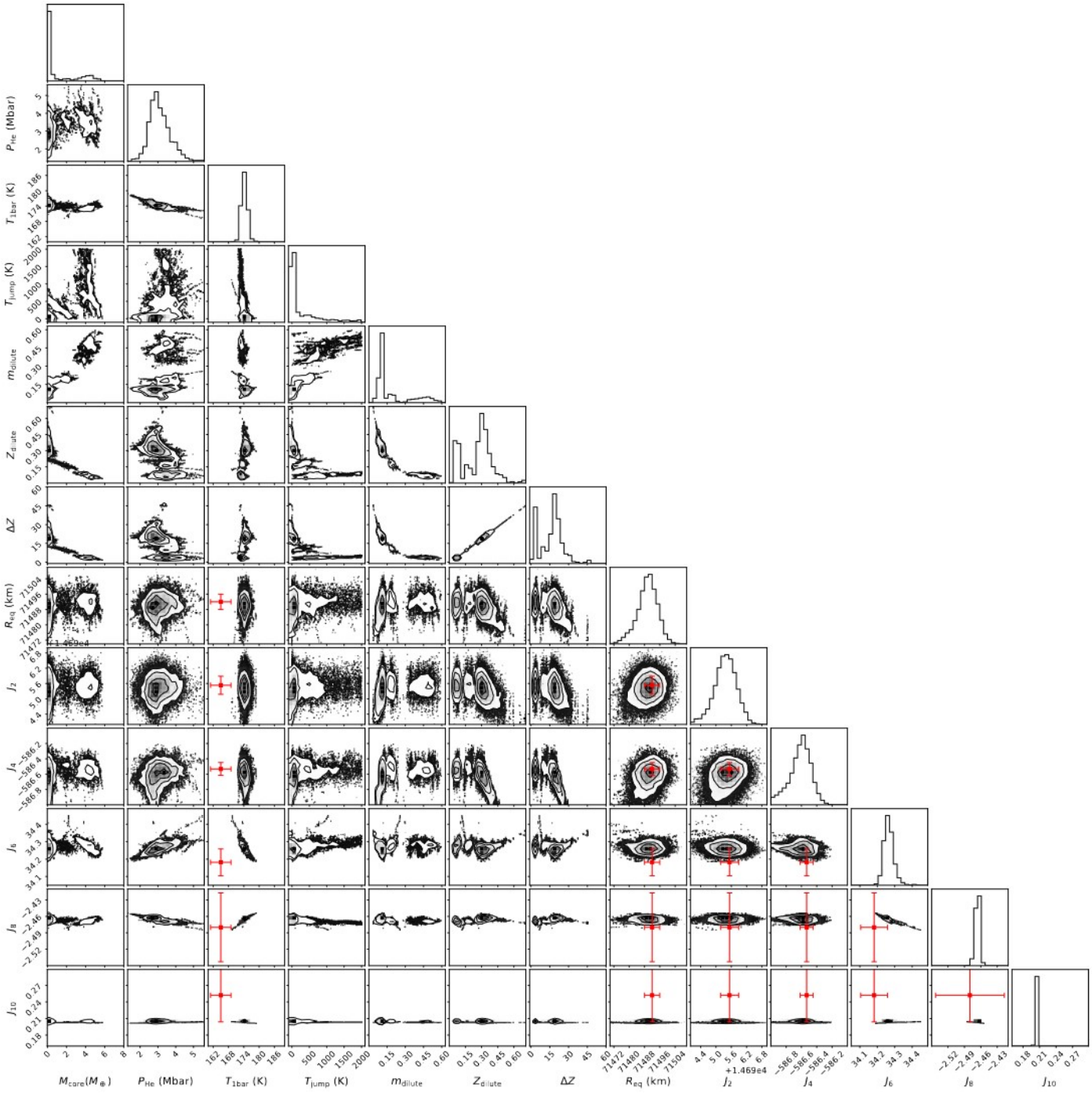

Fig. A.6: Resulting distributions obtained with the dilute-core model and the MLS20 equation of state.